# Spatial distribution of electron cloud footprints from microchannel plates: Measurements and modeling

A. S. Tremsin and O. H. W. Siegmund
*Experimental Astrophysics Group, Space Sciences Laboratory, University of California at Berkeley, Berkeley, California 94720*

(Received 13 October 1998; accepted for publication 21 April 1999)

The measurements of the electron cloud footprints produced by a stack of microchannel plates (MCPs) as a function of gain, MCP-to-readout distance and accelerating electric field are presented. To investigate the charge footprint variation, we introduce a ballistic model of the charge cloud propagation based on the energy and angular distribution at the MCP output. We also simulate the Coulomb repulsion in the electron cloud, which is likely to cause the experimentally observed increase in the cloud size with increasing MCP gain. Calculation results for both models are compared to the charge footprint sizes measured both in our experiments with high rear-field values (~200–900 V/mm) and in the experiments of Edgar *et al.* [Rev. Sci. Instrum. **60**, 3673 (1989)] (accelerating electric field ~30–130 V/mm). © *1999 American Institute of Physics.* [S0034-6748(99)04808-X]

## I. INTRODUCTION

Operation of microchannel plate (MCP)-based imaging detectors with charge-division readouts often requires optimization of the event charge footprint to achieve high spatial resolution and good image linearity. The best performance of many readout schemes is obtained when the charge cloud is spread out in the plane of the anode, so that several pitches of the repetitive electrode structure are covered. In fact, a narrow charge cloud can bring about an image distortion in the form of periodic modulation.[1] On the other hand, excessive spreading of the charge footprint leads to distortion at the image edges, thus reducing the effective area of the detector. For most charge-division readouts, where resolution depends on the charge division linearity, it is preferable to have a step-like profile for the charge spatial distribution instead of a superposition of a Gaussian-like central part and wide wings.[2–5] As suggested recently by Lapington,[6] a part of the wing component in such a distribution may be attributed to the secondary electron emission from the readout.

To achieve a better detector performance, the cloud footprint characteristics could be optimized by varying detector geometry and operational parameters. Edgar *et al.*[2] suggested a method for measuring the charge footprint profile at the anode and then studied these profiles for several detector configurations. Computer simulation could considerably reduce the amount of experimental measurements for optimization purposes. A substantial experience has been accumulated to date in simulation of such detector characteristics as MCP gain,[7] quantum efficiency,[8,9] thermal behavior,[10] temporal characteristics,[11] etc. However, the development of a feasible model for the charge cloud propagation has apparently been impeded by such factors as the statistical nature of the MCP output and the self-consistency of the electric field in the electron cloud. To our knowledge, only few results[12] on this matter have been reported so far. Zanodvorov *et al.*[12] presented a ''ballistic'' model of the charge cloud propagation based on the differential electron distributions at the MCP output, which had been measured in the experiments of Bronshteyn *et al.*[13] In this approach, no interactions between the electrons in the cloud are taken into account (the reason why this model can be called ballistic), i.e., the electric field is assumed to be constant rather than self-consistent. In the present paper (Sec. III A) we use a similar ballistic approach for simulating the charge footprint profile and compare the results with both our own experimental data (for high values of the MCP-anode accelerating field, ~200–900 V/mm) and the experimental results of Edgar *et al.*[2] (for low values of the rear electric field, ~30–130 V/mm).

However, with increasing MCP gain values the effects of Coulomb repulsion in the electron cloud may become more pronounced, thus requiring consideration. In Sec. III B, we present our attempt to estimate the contribution of the Coulomb repulsion to the charge cloud spreading. For this model, we also compare computation results with the experimental data of Edgar *et al.*[2] and our own (for low and high rear-field values, respectively).

## II. MEASUREMENTS

A stack of four back-to-back MCPs (40:1 L/D, 12 $\mu$m pore, 13$^o$ bias angle and 1 channel diameter end spoiling) was used in our measurements, Fig. 1. A P20 phosphor screen deposited onto a Schott fiberoptic (6 $\mu$m fiber) faceplate was positioned at 5 or 15 mm behind the stack. The input of the MCP stack was negatively biased. To produce a visible light output, a positive bias of 2500–4500 V was applied to the phosphor screen, providing a quasi-uniform accelerating electric field in the MCP-phosphor gap. The MCP gain was varied in the $3\times10^6$–$1.4\times10^7$ range. A pinhole mask with 50 $\mu$m diameter holes positioned 6 mm apart was placed in contact with the front surface of the input MCP, and a mercury vapor UV lamp (2537 Å) was used to illuminate the detector. Digital imaging was performed with

 © 1999 American Institute of Physics

Downloaded 24 Feb 2009 to 128.32.98.138. Redistribution subject to AIP license or copyright; see http://rsi.aip.org/rsi/copyright.jsp

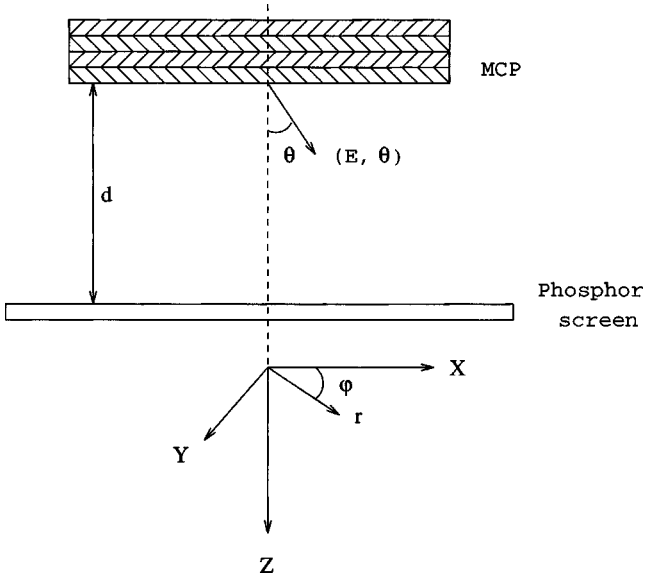


FIG. 1. Schematic diagram of the detector and the coordinate system used for calculations of the charge cloud spreading.

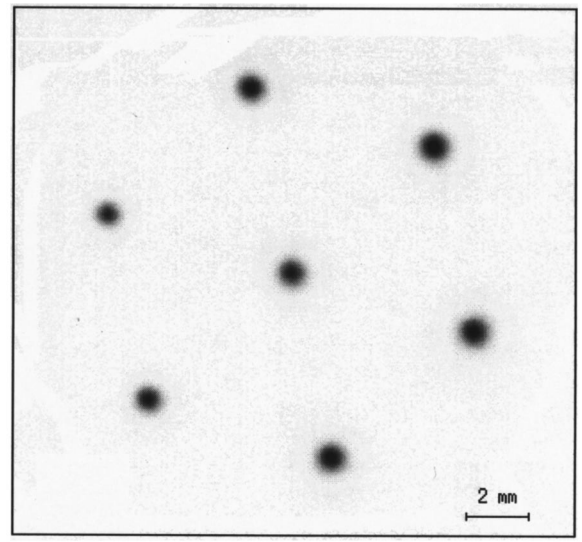


FIG. 2. Pinhole (50 $\mu$m) mask image obtained for a 5 mm phosphor-to-MCP stack gap, 4000 V accelerating bias and stack gain of $1.4\times10^7$. Distance between the spots is 6 mm.

a lens-coupled PULNIX TM-7CN CCD camera. The imaging spatial resolution of the screen and readout system was about 52 $\mu$m, dominated by the CCD pixel size. Figures 2 and 3 show a typical image and a histogram of a $\sim$50 $\mu$m wide section across it obtained at detector gain $1.4\times10^7$ with 5 mm gap between the phosphor screen and MCPs and a gap bias of 4000 V. Theoretically, one might expect the charge cloud shape to be nonsymmetric due to the presence of the MCP bias angle.[14] The resolution in our measurements was not sufficient for a detailed investigation of the charge cloud shape, as the footprint size was relatively small due to the high accelerating field between the MCP output and the phosphor screen. Therefore, we did not observe any dependence of the charge cloud footprints on the pore bias angle.

## III. CALCULATIONS

The statistical nature of the electron avalanche, originating at the output of the MCP channels, inhibits a precise calculation of the charge cloud evolution. The output electron angles and velocities exhibit large variations depending not only on the MCP intrinsic parameters (such as the length-to-diameter ratio L/D, the secondary electron emission coefficient of the semiconductive layer, the end spoiling, etc.), but also on the mode and sometimes even the history of operation. For instance, the saturated gain conditions are very different from the unsaturated mode of operation as reported elsewhere.[15,16] Besides, the long term gain depression phenomena,[17–19] as well as the local variation of MCP gain in the vicinity of a high count rate area,[10] also determine the manner in which the electron avalanche originates and develops. The abruptly changing electric fields at the pore exit impose yet more difficulties on the direct calculations. The Coulomb repulsion between the electrons in the cloud itself is difficult to describe precisely due to the presence in the process of a large number of particles with different velocity vectors. However, below we suggest some

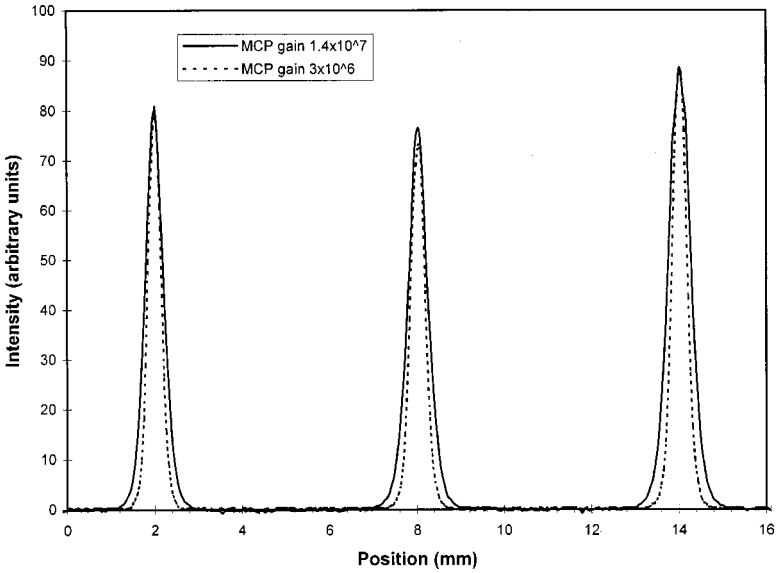


FIG. 3. Cross-sectional histograms ($\sim$50 $\mu$m wide) of the image shown in Fig. 2 and for the same setup with $3\times10^6$ gain.

Downloaded 24 Feb 2009 to 128.32.98.138. Redistribution subject to AIP license or copyright; see http://rsi.aip.org/rsi/copyright.jsp

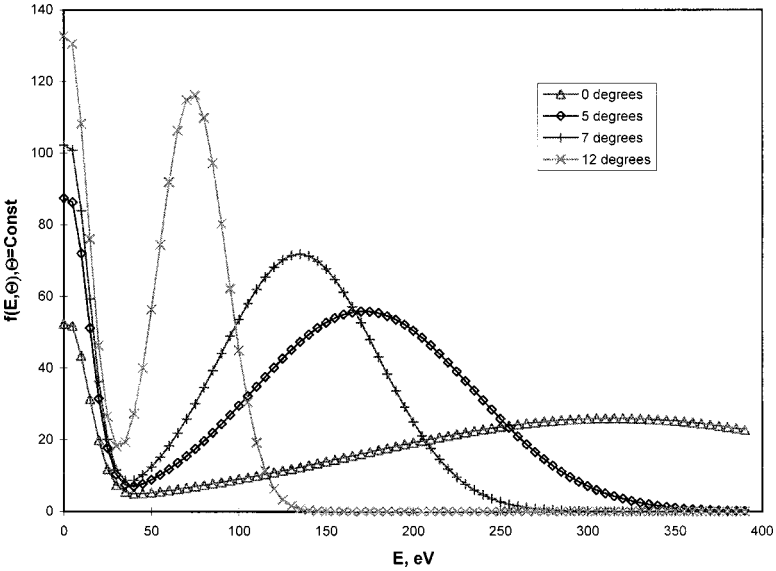


FIG. 4. Energy distribution curves of electrons at MCP output at fixed output angles, measured by Bronshteyn *et al.* (Ref. 13). 60:1 L/D MCP with 20 $\mu$m pores and one pore diameter end spoiling, $V_{\mathrm{MCP}}=1.4$ kV.

approximations which enable us to simulate the electron cloud development in the MCP-anode gap and obtain some information on the electron cloud footprint at the readout element of a detector.

### A. Ballistic model

Following the same approach as Zanodvorov *et al.*,[12] we assume the trajectories of all cloud electrons to be purely ballistic, and use the differential distribution function at the output of the MCP, measured by Bronshteyn *et al.*[13] (in fact, the results of Ref. 13 comprise the only available experimental data on that function, which is summarized in Fig. 4). It is assumed further that the distribution function represents the electron cloud which has been formed at some small distance from the MCP, where the electric field perturbations inflicted by the channel ends are negligible, and that starting from that point no interactions occur between the electrons in the cloud. Using the electron distribution function, it is possible to calculate the ballistic trajectories of all electrons and to estimate the cloud spatial distribution at any distance from the MCP. Ideally, the output distribution function should be measured separately for different MCP gain values, as this function may vary due to the Coulomb repulsion.

Figure 1 shows the coordinate system for our model described below. We use one of the experimental distributions of Ref. 13 (Fig. 4), which was measured with 1.4 kV MCP voltage on a single 60:1 L/D MCP with 20 $\mu$m pores. As was suggested previously,[12] the electron distribution function at the MCP output, obtained experimentally in Ref. 13, can be approximated by the following function:

$$f(E,\theta)=e^{-\tau^2/2\Delta^2}\left[A(\tau)e^{-(E-E_0)^2/2\sigma_0^2}-B(\tau)e^{-(E-E_1(\tau))^2/2\sigma_1^2(\tau)}\right], \tag{1}$$

where $E$ and $\theta$ are the electron output energy and angle, respectively, and $\tau=\tan(\theta)$. The unknown parameters in this distribution were chosen to fit the experimental data[13] and they have the form:

$$E_0=3\ \mathrm{eV},\ \sigma_0=12\ \mathrm{eV},\ \Delta=0.2,$$
$$A(\tau)=50.398e^{7.3822\tau},\ B(\tau)=25.992e^{9.8642\tau}, \tag{2}$$
$$E_1(\tau)=314.45e^{-6.9515\tau},\ \sigma_1(\tau)=147.62e^{-9.7077\tau}$$

In the present model, the function (1) is assumed to be symmetric, i.e., independent of the azimuthal angle $\varphi$. Therefore, the function of our interest—the radial distribution function at the plane of the anode (positioned at the distance $d$ from the plate), $\rho(r,\varphi)$, is also symmetric: $\rho(r,\varphi)\equiv\rho(r)$ and is defined as

$$2\pi\int_0^\infty \rho(r)r\,dr=1. \tag{3}$$

We introduce a transformation from variables $(E,\theta)$ to variables $(r,t)$—the radial distance from the emission point and time, thus

$$\int_0^\infty\int_0^\infty f(E,\theta)dE\,d\theta=\int_0^\infty\int_0^\infty f(E(r,t),\theta(r,t))\frac{\partial(E,\theta)}{\partial(r,t)}dr\,dt=1, \tag{4}$$

where $\partial(E,\theta)/\partial(r,t)$ is the Jacobian of the transformation.

The equation of motion of an electron in the cloud at the moment $t$ can be written as,

$$\begin{cases} r=\sqrt{\dfrac{2E}{m_e}}t\sin\theta, \\ d=\sqrt{\dfrac{2E}{m_e}}t\cos\theta+\dfrac{q_eUt^2}{2m_ed}, \end{cases} \tag{5}$$

where $d$ is the distance from the MCP, $U$ the accelerating bias in the MCP-anode gap, $q_e$ and $m_e$ are the electron charge and mass, respectively. Using Eq. (5), we obtain:

$$E(r,t)=\frac{m_e}{2}\left[\left(\frac{d}{t}-\frac{q_eUt}{2m_ed}\right)^2+\left(\frac{r}{t}\right)^2\right], \tag{6}$$

Downloaded 24 Feb 2009 to 128.32.98.138. Redistribution subject to AIP license or copyright; see http://rsi.aip.org/rsi/copyright.jsp

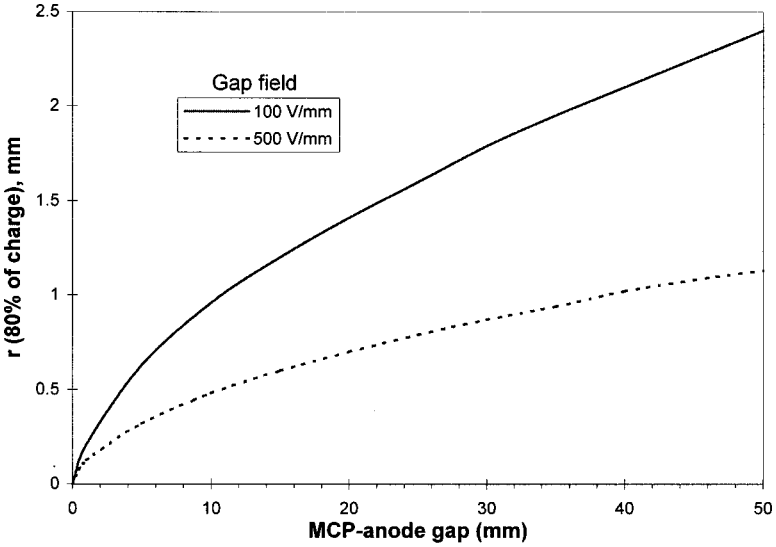


FIG. 5. Calculation results for the variation of the cloud size with MCP-to-readout distance and field (ballistic model).

$$\theta(r,t)=\arctan\left(\frac{r}{d-\frac{q_eUt^2}{2m_ed}}\right). \tag{7}$$

Then the Jacobian of variable transformation takes the form:

$$\frac{\partial(E,\theta)}{\partial(r,t)}=\frac{q_eU}{2dt}+\frac{m_ed}{t^3}. \tag{8}$$

Using two different expressions for the radial distribution function, Eqs. (3) and (4), and taking Eq. (8) into account, we obtain the following formula:

$$\rho(r)=\frac{1}{2\pi r}\int_0^\infty f(E(r,t),\theta(r,t))\left(\frac{q_eU}{2dt}+\frac{m_ed}{t^3}\right)dt. \tag{9}$$

Figure 5 shows the calculated dependence of the charge cloud size on the MCP-anode gap distance, Eq. (9), with the distribution function (1) and parameters (2) for the ballistic model. The calculated spatial charge cloud distributions $\rho(r)$ at different distances $d$ from MCP and gap bias $U$, are shown in Fig. 6. As seen from these results, variation of the accelerating bias changes mainly the size of the outer component (or the ''wing component,'' Ref. 1) of the charge cloud, consisting of the low energy electrons emitted at large angles.

As mentioned earlier, our ballistic model is based on the assumption that at some distance from the MCP the interaction between the electrons in the charge cloud becomes negligible, since the Coulomb repulsion weakens with the increase of the cloud size. Therefore, the validity of this model is provided by the fact that experimentally electron distribution function (1) can only be measured at some distance from the MCP.

### B. Coulomb repulsion

In this section, we consider how the Coulomb repulsion of the cloud electrons, determined by the spatial charge density, affects the charge cloud spreading. The repulsion process appears to be too complicated for an analytical description due to the spread of the pulse transit time and velocities of the electrons, which move in the self-consistent electric field, therefore some approximations will be introduced below.

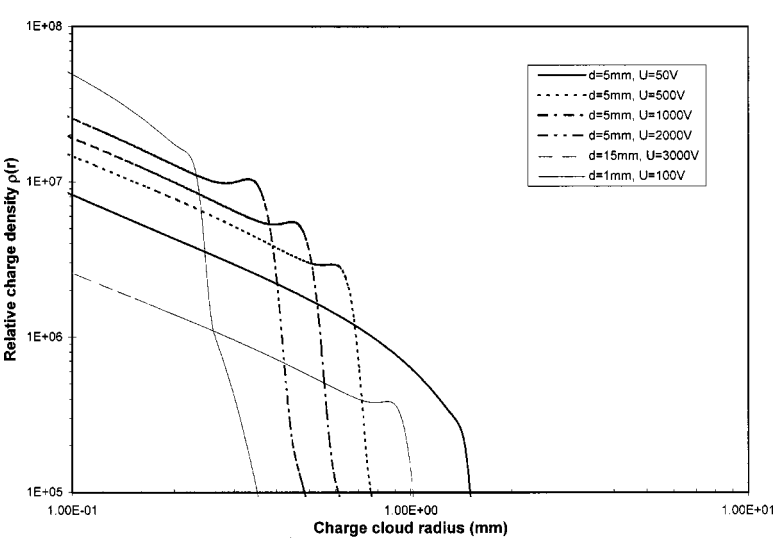


FIG. 6. Charge cloud distribution calculated with the ballistic model at different distances $d$ from the MCP and accelerating biases $U$.

Downloaded 24 Feb 2009 to 128.32.98.138. Redistribution subject to AIP license or copyright; see http://rsi.aip.org/rsi/copyright.jsp

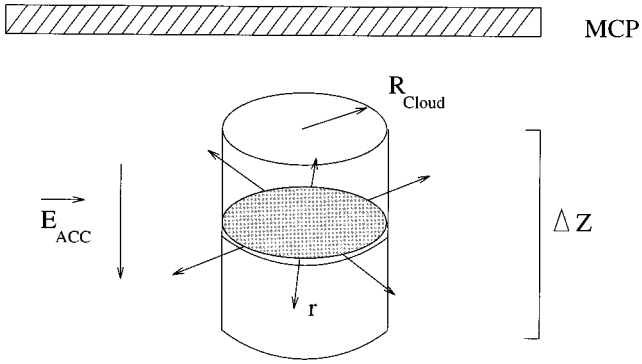


FIG. 7. Schematic diagram of the coordinate system used in the Coulomb repulsion model and the charge cloud spread.

The Monte Carlo technique successfully used by Jansen[20] for the modeling of charged particle beams, is very difficult to apply in this case due to a very large number of interacting particles, and the problem cannot be simplified by the two-body scattering approach as suggested by Beck *et al.*[21] We presume that each electron in the cloud moves in the electric field formed by two components: the accelerating field $\vec{E}_{\mathrm{acc}}$ of the bias in the gap, and the macroscopic field imposed by the rest of the electron cloud $\vec{E}_{\mathrm{Coulomb}}$. We suppose also that all electrons are emitted from the MCP at a normal angle and that at the moment $t_0$ they are uniformly distributed in the *XY* plane of the active area, i.e., the initial spatial distribution of electrons in that plane is uniform and concentrated within a cylinder with radius $R^0_{\mathrm{cloud}}$: $\rho(r,\varphi,t) \equiv \rho(r,t)$ and $\rho(r,t)|_{t=t_0} \equiv \rho(r,t_0) \equiv \mathrm{Const}$, $r \leqslant R_{\mathrm{cloud}}|_{t=t_0} \equiv R^0_{\mathrm{cloud}}$ (Fig. 7).

Another assumption that we use deals with the *z* spread of the charge cloud due to the pulse transit time spread, which, according to Ref. 7, is proportional to $\sim\sqrt{V_{\mathrm{MCP}}}$ and is of the order of 50 ps for a typical chevron stack. However, the charge footprint at the readout element comprises a projection of the charge cloud onto the plane of the anode, therefore a particular purpose of the current simulation is to describe the charge spreading in *XY* plane. We divide the charge cylinder into virtual disks and then simulate the electron repulsion within a disk, Fig. 7 (assuming that within that disk the repulsion along *Z* axis is negligible), thus limiting ourselves to solving a two-dimensional problem. To specify the portion of the total charge confined within such a virtual disk, we introduce a parameter $A = Q_{\mathrm{disk}}/Q_{\mathrm{total}}$. Hence, we use the initial condition for the radial charge distribution in the form:

$$\rho(r,t_0) = \frac{Q_{\mathrm{disk}}}{\pi R^2_{\mathrm{cloud}}} = \frac{A Q_{\mathrm{total}}}{\pi R^2_{\mathrm{cloud}}}. \tag{10}$$

The equations of a single electron motion between the MCP output and readout are as follows:

$$m_e \ddot{r}(t) = q_e \cdot E_{\mathrm{Coulomb}}(r,t), \tag{11}$$

$$m_e \ddot{z}(t) = q_e \cdot E_{\mathrm{acc}}, \tag{12}$$

where $[r(t),z(t)]$ are individual electron trajectories, $q_e$ and $m_e$ are the electron charge and mass, $E_{\mathrm{acc}}$ is the accelerating field and $E_{\mathrm{Coulomb}}(r,t)$ can be calculated from equation:

$$E_{\mathrm{Coulomb}}(r,t) = \frac{Q}{4\pi\varepsilon_0}\int_0^{\infty}\int_0^{2\pi}\frac{\rho(\xi,t)}{2\pi} \cdot \frac{r-\xi\cos\varphi}{(\xi^2+r^2-2\xi r\cos\varphi)^{3/2}}\xi d\xi d\varphi. \tag{13}$$

Equations (11)–(13) comprise a nonlinear system since individual electron trajectories depend on the electron distribution function which, in turn, changes with the electron motion.

If the solution of Eqs. (11)–(13) with initial conditions (10) is known (i.e., the electron trajectories are defined), then for each electron in the cloud the position at the moment $t^{i+1}$ is determined by its position at the moment $t^i$. We introduce a function $F[r(t)]$ to describe this relationship:

$$r(t^{i+1}) = F[r(t^i)], \Rightarrow r(t^i) = F^{-1}[r(t^{i+1})], \tag{14}$$

where $F^{-1}$ is the inverse function to $F$, which exists as function $F$ is single valued (since for our initial conditions the distance between any two electrons in the cloud increases with time). We can write the charge conservation equation for $r(t^i) \in [0,\infty)$ as

$$\int_0^{r(t^{i+1})} \rho(\xi,t^{i+1})\xi d(\xi) = \int_0^{r(t^i)} \rho(\xi,t^i)\xi d(\xi). \tag{15}$$

By differentiating Eq. (15) and taking Eq. (14) into account, we obtain the following formula:

$$\rho(r,t^{i+1}) = \rho(r,t^i)\frac{r(t^i)}{r(t^{i+1})}\frac{dF^{-1}[r(t^{i+1})]}{dr(t^{i+1})}, \tag{16}$$

where $\rho(r,t^i)$ is the spatial distribution at the moment $t^i$.

The solution of Eqs. (11)–(13), (16), with initial conditions (10), can be obtained numerically as follows. For the initial moment $t = t_0$, we introduce a logarithmically spaced grid $\{r^0_0,\ldots r^0_N\}, r^0_N = R^0_{\mathrm{cloud}}$. By solving Eq. (12), we can find the time $T_{\max}$ when the cloud reaches the anode positioned at distance d:

$$T_{\max} = \sqrt{2E_0 m_e}\,\frac{\sqrt{1+\dfrac{q_e E_{\mathrm{acc}} d}{E_0}}-1}{q_e E_{\mathrm{acc}}}. \tag{17}$$

Then for each time step $t^i = t^{i-1} + \Delta t^i$, we follow the scheme:

(1) We obtain $E_{\mathrm{Coulomb}}(r^{i-1}_j, t^i)$ by the numerical integration of Eq. (13) with $\rho(\xi,t) = \rho(\xi,t^{i-1})$.

(2) We assume that for $t \in [t^{i-1},t^i]$: $E_{\mathrm{Coulomb}}(r,t) \equiv E_{\mathrm{Coulomb}}(r^{i-1}_j, t^{i-1}) \equiv \mathrm{Const}$. By integrating Eq. (11) with the known values from the previous time step $r^{i-1}_j$ ($j = 0,\ldots N$), we find $r^i_j$ ($j = 0,\ldots N$).

(3) We use the discrete analogue of Eq. (16) in the form:

$$\rho(r^i_j) = \rho(r^{i-1}_j)\frac{r^{i-1}_j}{r^i_j} \cdot \frac{r^{i-1}_j - r^{i-1}_{j-1}}{r^i_j - r^i_{j-1}}, \tag{18}$$

($j = 0,\ldots N$), to obtain the discrete distribution function values for the time step i.

Downloaded 24 Feb 2009 to 128.32.98.138. Redistribution subject to AIP license or copyright; see http://rsi.aip.org/rsi/copyright.jsp

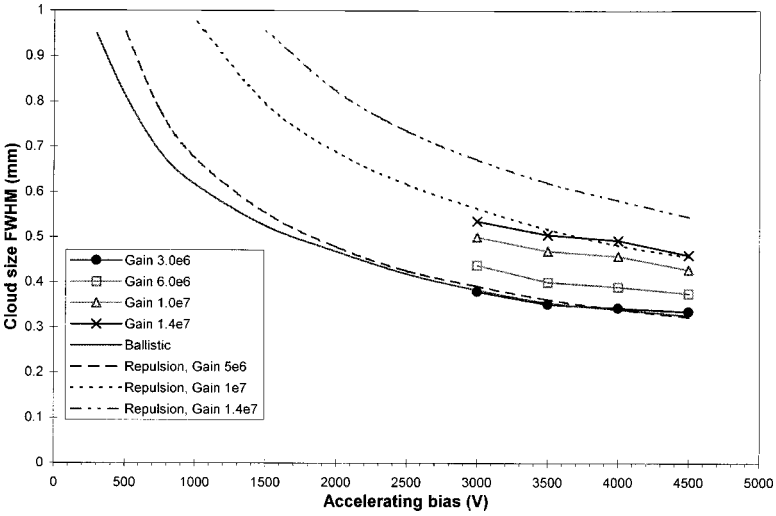


FIG. 8. Variation of the charge cloud size for a 5 mm phosphor-MCP gap with accelerating bias. ●, □, △, ×—measured with the phosphor screen and gains $3.0\times10^6$, $6.0\times10^6$, $1.0\times10^7$, and $1.4\times10^7$, respectively; solid line—ballistic calculations; dashed/dotted lines—Coulomb repulsion calculations with $A=0.02$, $R_{\mathrm{cloud}}=75$ $\mu$m and gains $5.0\times10^6$, $1.0\times10^7$, and $1.4\times10^7$.

Steps (1)–(3) are repeated until $t^i$ reaches $T_{\max}$. The calculation process starts with a small time increment $\Delta t^0=0.5$ ps, and then for the purposes of computing efficiency, we increase $\Delta t^i$ in geometrical progression (with factor 1.04), as the Coulomb repulsion decreases with charge propagation. A typical value of $N=100$ was used in our computations.

## IV. RESULTS AND DISCUSSION

Figure 8 compares the results of our measurements and calculations of the electron cloud size at 5 mm from the MCP stack. The ballistic calculations correlate well with the measured data for MCP gain of $3\times10^6$ and accelerating biases 3000–4500 V across the gap, although due to the phosphor cutoff no measurement results were available for lower accelerating biases for the same MCP stack. The cloud size increases with the increase of MCP gain, therefore the coefficients (2) of the output distribution function (1), used in the ballistic model, should vary with MCP gain increase.

As mentioned above, $A$ (10) is the only parameter in our repulsion model which needs to be adjusted to experimental data. Our calculations showed that the parameter $A$ of about 2% of the total charge yields a relatively good agreement between the results of calculations and our measurements. As seen in Fig. 8, simulation results for the cloud size increase solely due to the Coulomb repulsion are reasonably consistent with the measured data, and they are also close to the results of ballistic calculations for a low gain. However, for gains higher than $10^7$, the contribution of the Coulomb repulsion, calculated with the same parameters as for lower gains, appears overestimated. This can probably be corrected by adjusting the model parameter $A$ (10), as the increase of the pulse transit time spread and the variation of the output energy distribution should result in lower values of that parameter. Figure 9 shows the results of measurements and calculations for the 15 mm gap (with the same set of model parameters as in the case of 5 mm gap).

We also evaluated our calculations in the range of lower accelerating biases by comparing them with the detailed spatial distribution measurements reported by Edgar *et al.*,[2] who used a chevron stack with a 100 $\mu m$ gap, no bias between the 80:1 L/D 36 mm diameter plates and the end spoiling of half a pore diameter (as opposed to one pore diameter in our measurements), Fig. 10. A split strip anode was positioned 6.2 mm behind the stack. We used the same value of $A=0.02$ in these calculations of the Coulomb repulsion con-

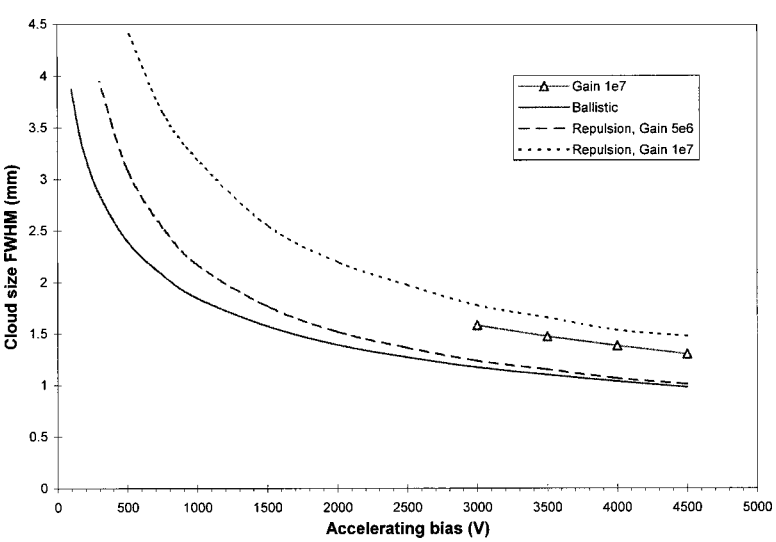


FIG. 9. Variation of the charge cloud size for a 15 mm phosphor-MCP gap with accelerating bias. △—measured with the phosphor screen and gain $1.0\times10^7$; solid line—ballistic calculations; dashed/dotted lines—Coulomb repulsion calculations with $A=0.02$, $R_{\mathrm{cloud}}=75$ $\mu$m and gains $5.0\times10^6$, and $1.0\times10^7$.

Downloaded 24 Feb 2009 to 128.32.98.138. Redistribution subject to AIP license or copyright; see http://rsi.aip.org/rsi/copyright.jsp

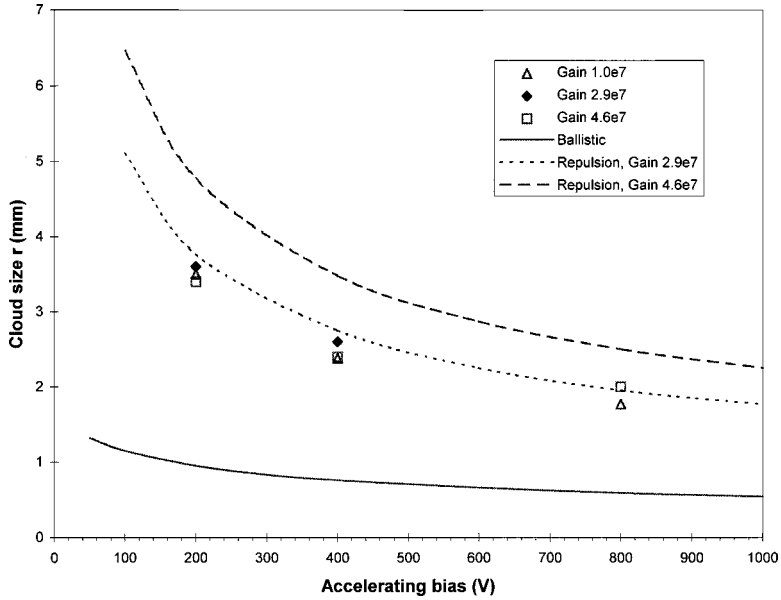


FIG. 10. Variation of the charge cloud size $r$ for a 6.2 mm anode-to-MCP gap with accelerating bias. 80% of total charge is constrained within radius r. △, ◇, □—measurements by Edgar *et al.* (see Ref. 2) with the chevron stack of 36 mm in diameter, 80:1 L/D MCPs, 100 $\mu m$ gap and no bias between the plates, the end spoiling of half a pore diameter, gains $1.0\times10^7$, $2.9\times10^7$, and $4.6\times10^7$, respectively. Solid line—ballistic calculations; dashed/dotted lines—Coulomb repulsion calculations with $A=0.02$, $R_{\mathrm{cloud}}=50$ $\mu$m and gains $2.9\times10^7$, and $4.6\times10^7$.

tribution, as for the modeling of our measurements. In this case, the value $R_{\mathrm{cloud}}$ corresponds to the active area of the second MCP, and it is equal to the size of the electron cloud footprint at the input surface of the second MCP. $R_{\mathrm{cloud}}$ was then calculated ballistically (Sec. III A) with Edgar's setup parameters and the distribution (1) and was found to be 50 $\mu$m. Not surprisingly, our ballistic calculations, based on the data of Bronshteyn *et al.*[13] for the end spoiling of one pore diameter, yield lower values of the cloud size than can be expected for the end spoiling of half a pore diameter in Edgar's experiments. In the latter case, the electrons are emitted in a wider angle, therefore the coefficients (2) in the distribution function (1) should be corrected for a smaller end spoiling. Our estimate of the repulsion contribution is also in a good agreement with Edgar's data for $2.9\times10^7$ gain, although no substantial increase in the cloud size was observed in those experiments with the fourfold increase in the gain.

Summarizing the above comparisons, we can conclude that the results of our calculations can be used for estimating the charge cloud size for different detector operation parameters, in particular MCP-to-anode distance, accelerating electric field and MCP gain. Optimization of these parameters for a particular detector configuration may result in a substantial improvement of detector uniformity and spatial resolution. The models presented above should be used in conjunction with experimental calibrations necessary for their adjustment. Once the parameters are established, the model can provide results for a number of operating conditions, thus reducing the amount of calibration required for detector optimization. Our ballistic model provides not only the size of the charge cloud at a given distance, but also its shape, which is important for many charge division readouts. The future work will include a more detailed study of the charge footprint nonsymmetry, caused by the MCP channel tilt, and its influence on the spatial resolution. Besides, direct measurements of the MCP output distribution function (1) for different MCP end spoiling values and operational parameters could provide very useful data for the ballistic model applications.

## ACKNOWLEDGMENTS

The authors would like to thank Dr. M. L. Edgar for the helpful comments and our colleagues at Experimental Astrophysics Group for their support of the measurements. AST is also grateful to Dr. I. D. Rodionov for the useful discussions of the ballistic model.

[1] J. V. Vallerga, G. C. Kaplan, O. H. W. Siegmund, M. Lampton, and R. F. Malina, IEEE Trans. Nucl. Sci. **NS-36**, 881 (1989).
[2] M. L. Edgar, R. Kessel, J. S. Lapington, and D. M. Walton, Rev. Sci. Instrum. **60**, 3673 (1989).
[3] J. S. Lapington and M. L. Edgar, Proc. SPIE **1159**, 565 (1996).
[4] J. S. Lapington, R. Kessel, and D. M. Walton, Nucl. Instrum. Methods Phys. Res. A **273**, 663 (1988).
[5] M. L. Edgar, Ph.D. thesis, University of London, 1993.
[6] J. S. Lapington, Nucl. Instrum. Methods Phys. Res. A **392**, 336 (1997).
[7] G. W. Fraser, Nucl. Instrum. Methods Phys. Res. A **291**, 595 (1990).
[8] G. W. Fraser, Nucl. Instrum. Methods Phys. Res. **206**, 445 (1983).
[9] P. M. Shikhaliev, Rev. Sci. Instrum. **68**, 3676 (1997).
[10] A. S. Tremsin, J. F. Pearson, G. W. Fraser, W. B. Feller, and P. B. White, Nucl. Instrum. Methods Phys. Res. A **379**, 139 (1996).
[11] M. Ito, H. Kume, and K. Oba, IEEE Trans. Nucl. Sci. **NS-31**, 408 (1984).
[12] N. P. Zanodvorov, N. K. Zolina, A. M. Tyutikov, and Yu. A. Flegontov, Radio Eng. Electron. Phys. **25**, 129 (1980).
[13] I. M. Bronshteyn, A. V. Yevdokimov, V. M. Stozharov, and A. M. Tyutikov, Radio Eng. Electron. Phys. **24**, 150 (1979).
[14] A. S. Tremsin, J. V. Vallerga, and O. H. W. Siegmund, to appear in Nucl. Instrum. Methods Phys. Res. A, Proceedings of 5th International Conference on Position-Sensitive Detectors, London, September 1999.
[15] N. Koshida and M. Hosobuchi, Rev. Sci. Instrum. **56**, 1329 (1985).
[16] N. Koshida, Rev. Sci. Instrum. **57**, 354 (1986).
[17] A. S. Tremsin, J. F. Pearson, J. E. Lees, G. W. Fraser, W. B. Feller, and P. White, Proc. SPIE **2808**, 86 (1996).
[18] M. L. Edgar, J. S. Lapington, and A. Smith, Rev. Sci. Instrum. **63**, 816 (1992).
[19] J. S. Lapington, M. L. Edgar, and A. Smith, Proc. SPIE **1743**, 283 (1996).
[20] G. H. Jansen, *Coulomb Interactions in Particle Beams* (Academic, San Diego, 1990).
[21] V. Beck, M. Gordon, and T. Groves, J. Vac. Sci. Technol. B **7**, 1438 (1989).

Downloaded 24 Feb 2009 to 128.32.98.138. Redistribution subject to AIP license or copyright; see http://rsi.aip.org/rsi/copyright.jsp